CrossMark

Polarization and QPOs from jets in black hole systems

A. MANGALAM

Indian Institute of Astrophysics, 2nd Block Koramangala, Bengaluru 560 034, India.
E-mail: mangalam@iiap.res.in

Abstract. The historical observations of polarized jet emission for Blazars are reviewed and previous models are discussed. Motivated by this, a model for polarization of both steady and transient behavior using a helical magnetic field is presented. The variety of observed correlations and anti-correlations between the electric polarization angle, the degree of polarization and optical flux can be explained by this model. In addition, the phenomena of quasi-periodic oscillations (QPO) behavior seen in jets in X-ray Binaries (XRBs) is also explained by a model based on helical trajectories of emitting blobs and the resulting time scales and harmonics of the QPO are derived. In both the models, the input parameters are the inclination angle, the Lorentz factor of the jet and pitch angle of the magnetic helix.

1. Introduction

There have been several multi-wavelength detections of jet polarization and related flux variations in the literature and various models have been proposed; we discuss the prominent detection and associated models here.

With the help of sequences of high-resolution radio images and optical polarization measurements of the blazar BL Lacertae, Marscher *et al.* (2008) observed a bright feature in the jet that causes a double flare of radiation from optical bands to TeV X-ray energies, as well as a delayed outburst at radio wavelengths. The feature brightens again as it appears to cross a standing shock wave corresponding to the bright core seen on the radio images. The observations of the source 3C279 by Abdo *et al.* (2010) showed that the visible-light polarization changed drastically during the giant 20-day γ-ray flare. There is a nexus established between the the γ-ray and visible-light emission regions, showing that they emerge from essentially the same location. Also, the varying polarization properties are indicative of a blob motion in the jet; for example, the changing angle between the direction of the blob's motion and our line of sight can reproduce the observed changes in the angle and degree of polarization.

Many multi-band observations of 3C 454.3 have been conducted, including recent simultaneous γ-ray incorporating Fermi/AGILE data. For example, in Bonning *et al.* (2009), good correlations between IR, optical, UV and γ-ray fluxes were seen, with lags within a day. The X-ray flux was almost flat and not correlated with either the higher or lower frequency measurements. Vercellone *et al.* (2009) also observed correlated optical and high-energy γ-rays using AGILE, but the INTEGRAL and Swift X-ray measurements were not well correlated. Nearly simultaneous flux peaks across all bands from mm to γ-rays during the strong flares were found with complete AGILE-led multi-band monitoring of 3C 454.3 over 20 months (Vercellone *et al.* 2010; Raiteri *et al.* 2011), with the γ–optical correlation usually having a time-lag less than a day. Good correlations between γ-ray and optical light curves (LCs) were found (Gaur *et al.* 2012a), although the γ-ray LC led the optical one by 4.5 ± 1.0 days.

Gupta *et al.* (2017) analyzed the strong flare from blazar 3C454.3 seen in γ-rays, X-rays, and optical/NIR bands during $3-12$ December 2009. The emission in the V and J bands increased more gradually than did the γ-rays and soft X-rays, however all peaked at nearly the same time. Optical polarization changed largely during the flare, with a strong anti-correlation between optical flux and degree of polarization (which increased from $\sim 3\%$ to $\sim 20\%$) during the declining phase of the flare. The flare also had by large and quick changess in

polarization angle of $\sim 170°$. This combined behaviors appears to be distinct.

Blazar light curves show quasi-periodic variability over a diverse range of time-scales: ~ 100 s to a few 100 s in the γ-rays (e.g. Aharonian *et al.* 2007); ~ 1000 s to a few hours in the optical/UV and X-rays (e.g. Böttcher *et al.* 2003; Lachowicz *et al.* 2009); intra-day variability in the optical (e.g. Gaur *et al.* 2012b and references therein) and radio (e.g. Liu *et al.* 2013), short time-scale variability of a few days to weeks in optical (e.g. Gaur *et al.* 2012a and references therein) and months to years in the optical and radio (e.g. Mohan & Mangalam 2015). Disk based models have been proposed to explain the X-ray variability and QPOs and the associated data analysis have been discussed for AGN (Mohan & Mangalam 2014; Mohan *et al.* 2011).

Similarly, for the case of black hole X-ray binaries (BHXRB), there are QPOs that are thought to be associated with jets. For example, Type-B QPOs which are usually observed during soft intermediate state, when the hard to soft spectral transition is taking place, and can coincide with the occurrence of jets (Fender *et al.* 2009). Type-C QPOs are the most common type and can occur in any spectral state, but usually observed during low hard state (at the beginning of an outburst) or in the hard intermediate state (Motta *et al.* 2012). The jets are present in the beginning of outburst (Fender & Belloni 2012). Almost all the sources like GROJ1655-40, XTE J1550-564, GX 339-4, H1743-322 and GRS 1915+105 are known to have shown these QPOs (Motta 2016).

In this paper, we review previous models in section 2, discuss previous kinematic proposals in section 3, the degree of polarization in section 4, and in section 5, we present a new double helix model and calculate the polarization profiles. In section 6, we calculate the harmonics and its amplitude ratios of QPOs that is attributed to a helical jet and present our conclusions in section 7. A glossary of symbols used is provided in Table 1.

2. A review of previous approaches to polarization

Lyutikov *et al.* (2005) studied the steady polarization properties of optically thin synchrotron radiation emitted by relativistically moving electron-positron jets carrying large-scale helical magnetic fields. The jet is taken to be cylindrical and the emitting plasma moves along to the jet axis with a Lorentz factor Γ. Their calculations show the following behavior. For jets unresolved in the direction perpendicular to their direction of propagation, the position angle of the electric vector

Table 1. Glossary of symbols.

Geometrical parameters	
θ	Inclination angle
n	Unit vector pointing to observer
l	Unit vector normal to plane containing $\hat{z}$ and **n**
w	$w/\sqrt{w^2+1} = \tan\delta$
δ	Pitch angle
Kinematic parameters	
g	General relativistic Doppler effect
$\mathcal{D}$	Special relativistic Doppler effect
r_J	Jet radius
v	Velocity of the emitter
Γ	$1/\sqrt{1-\beta^2}$ where $\beta = v/c$
Emission and polarization parameters	
p	Power law index of the particle energy distribution ϵ^{-p}
Π	Degree of polarization
χ'	Rest frame viewing angle
$\tilde{\chi}$	Observed EVPA (electric vector polarization angle)
e	Direction vector of the electric field of the emission
ζ	Angle between the electric and magnetic fields
λ	Power of the Doppler factor in the intensity

(EVPA) of the linear polarization is found to be either parallel or perpendicular to the jet. They conclude that large-scale magnetic fields can explain the key polarization properties of parsec-scale AGN jets. The typical degrees of polarization (DOP) are $\leq 15\%$, which indicate that the rest-frame toroidal and poloidal fields are similar in strength. The most relativistic jets are overwhelmed by the toroidal magnetic field component in the observed frame with $B_\phi/B_z \sim \Gamma$.

Marscher *et al.* (2008) showed that the optical flux and polarization variability in BL Lac seen in 2005, which included a large swing in the EVPA coincident with rapid changes in the DOP, is explained in terms of a shock wave leaving the vicinity of the central black hole and propagating down only a portion of the jet's cross section. In this case, the disturbance follows a spiral path in a jet that is both accelerating and becoming more collimated. This interpretation is supported for that flare by the presence of a bright superluminal knot

in their VLBA radio maps and the agreement between the optical and 7 mm radio polarization directions.

Larionov *et al.* (2013) suppose, following Marscher *et al.* (2008), that most of optical photometric and polarimetric variability arises when a compact emission region (e.g., a shock wave) propagates downstream from the black hole, following a spiral path. Alternatively, the jet could have a helical geometry. Prominent optical outbursts are quite often both preceded and followed by minor flares. They interpret this phenomenon as a manifestation of the oscillating Doppler beaming of the emission using the lighthouse effect (Camenzind & Krockenberger 1992). The observed series of outbursts correspond to the time intervals when the viewing angle of the shock wave is at a minimum.

In many of the previous observations of blazars including polarimetry (e.g., Marscher *et al.* 2008; Sasada *et al.* 2010; Marscher *et al.* 2010; Jorstad *et al.* 2010), a smooth change of the polarization angle with the rise in optical flux has been seen on long term observations. This can be understood as due to a non-axisymmetric magnetic field distribution, motion of the jet across our line of sight, or a curved trajectory of the dissipation/emission pattern (Konigl and Choudhuri 1985; Gopal-Krishna and Wiita 1992; Marscher *et al.* 2008). It also may be due to the propagation of a knot of emission that follows a helical path in a magnetically dominated jet, as considered in the context of the event seen in BL Lac in long term observations in 2005–2006 (Marscher *et al.* 2008). The large swings of polarization can be due to bending jet models where the angle the jet makes with our line of sight changes (e.g., Gopal-Krishna92). If variability arises from helical structures, the observed polarization can be calculated following Lyutikov *et al.* (2005) and Raiteri *et al.* (2013).

Calculations of X-Ray and gamma-ray polarization in leptonic and hadronic Blazar models involve synchrotron polarization ($p\gamma$ or $e\gamma$ interactions) with the standard description for the degree of polarization

$$\Pi = \frac{p+1}{p+7/3}, \quad \text{for } p = 2, \Pi = 0.69$$
$$\text{and for } p = 3, \Pi = 0.75. \quad (1)$$

where p is the power law index in the energy distribution, ϵ^{-p}.

A model for synchrotron polarization in blazars, involving three-dimensional radiation transfer and assuming a standard shock-in-jet explanation for the flare in a jet with an originally dominant helical magnetic field, recently has been developed (Zhang *et al.* 2014, 2015). These simulations can reproduce the range
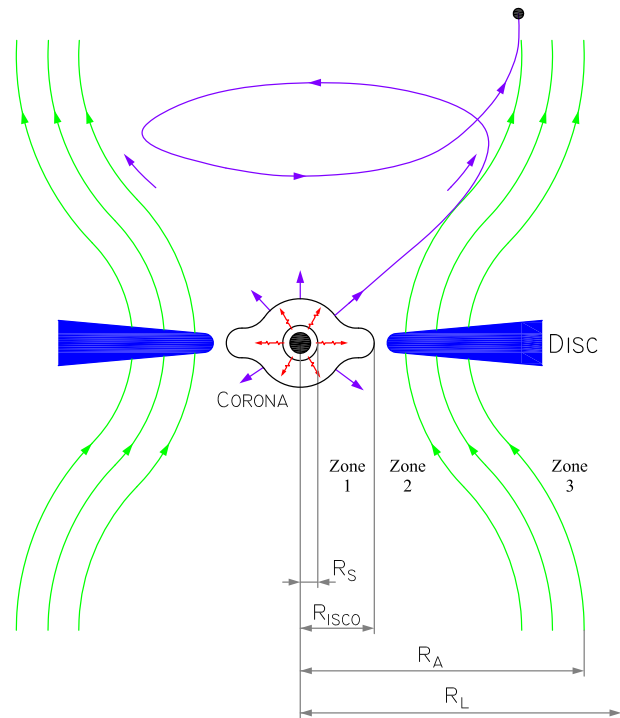
Figure 1. A blob is launched in Zone 1 driven by radiation pressure, centrifugally driven in Zone 2 and it reaches final angular momentum. Quasi periodic variability is produced due to the orbital motion of blob along a helical path as the local angle is close to the observer's line of sight. Courtesy: MM15.

of polarization behaviors seen during earlier flares without requiring either bent or helical jet trajectories.

3. Kinematic inputs for polarization models

After reviewing several models we narrow down on a possible kinematic inputs for models to explain the flare events seen in multi-wavelength campaigns along with the polarization properties.

One approach, perhaps a simple but likely case, involves taking a blob equivalent to that of a mini-jet having a constant rest frame emission and polarization properties that is following a bent helical path. Mohan and Mangalam (2015) (MM15) present a general relativistic model of jet variability in active galactic nuclei due to orbiting blobs in helical motion along a funnel or cone shaped magnetic surface anchored to the accretion disk near the black hole (see Fig. 1). The simulated light curves (LCs) for the funnel model include Doppler and gravitational shifts, aberration, light bending and time delay are produced by calculating the *g* factor. The beamed intensity has a systematic phase shift with

respect to that from a previous special relativistic model (Camenzind & Krockenberger 1992). The results justify implementing a realistic magnetic surface geometry in a GR framework to describe effects on emission from orbital features in the jet close to the horizon radius. In the model, the varying GR Doppler factor (defined as the ratio of received and emitted photon energies) is given by

$$g = \frac{E_{\text{rec}}}{E_{\text{em}}} = \frac{(1 - 2r_{\text{g}}/r)^{1/2}}{\Gamma(1 - \beta_\Gamma \cos\xi)} \quad (2)$$

where $\xi(t)$ is angle between the photon velocity unit vector and the emitter's velocity vector, $\beta_\Gamma = (1 - \Gamma^{-2})^{1/2}$, Γ is the Lorentz factor, and the time interval in observer frame $d\tilde{\tau}$ in relation to coordinate time interval dt is given by

$$\tilde{\tau} = (1 + \tilde{z}) \int_0^t dt (1 - \beta_\Gamma \cos\xi). \quad (3)$$

The light curve is given by the spectral flux density observed $F_\nu(t)$. If F_ν' is the spectral flux density in the co-moving frame, these are related by the expression

$$F_\nu(\tilde{\tau}) = g^\lambda(t) F_\nu'(\tilde{\tau}), \quad (4)$$

where $\lambda = 3 + \alpha$ for a resolved blob of plasma and $\lambda = 2 + \alpha$ for a continuous flow; where α is the spectral index which is the slope in the relation $F_\nu \propto \nu^\alpha$ between the spectral flux F_ν and the emission frequency in the observer frame. Either case of λ is possible depending on the particular application to observations.

The input model parameters are λ, Γ, the inclination angle θ, the specific angular momentum j, knot launch radius ϖ_0 while the knot trajectory is given by $x_s = (\varpi \cos\phi, \varpi \sin\phi, z)$, where the beaming angle is

$$\cos\xi = \frac{\dot{\varpi} \cos\phi \sin\theta - \varpi \dot{\phi} \sin\phi \sin\theta + \dot{z} \cos\theta}{(\dot{\varpi}^2 + \varpi^2\dot{\phi}^2 + \dot{z}^2)^{1/2}} \quad (5)$$

where (ξ, F_ν) as a function of $z(\tilde{\tau})$ (from invariant four-velocity relation $u^\beta u_\beta = -c^2$) is calculated from

$$\frac{\dot{z}}{c} = r(1 - 2r_{\text{g}}/r)$$

$$\left(\frac{1 - (1 - 2R_{\text{g}}/r)\left(\Gamma_F^{-2} + \frac{j^2}{\varpi^2 c^2}\right)}{(\varpi \tan\theta_0 + z)^2 + (1 - 2r_{\text{g}}/r)\varpi_0^2} \right)^{1/2} \quad (6)$$

$$\Gamma = \Gamma_F (1 - 2r_{\text{g}}/r)^{-1/2} \quad (7)$$

where Γ_F is the asymptotic Lorentz factor. The above helical jet model of MM15 has been successfully applied to explain the kinematics of PG 1302-102 (Mohan *et al.* 2016) and CTA 109 (Li *et al.* 2018).

The quasar PG 1302-102 is believed to harbor a supermassive binary black hole (SMBBH) system. Using the available 15 GHz and 2−8 GHz, multi-epoch Very Long Baseline Array data, Mohan *et al.* (2016) constrain the pc-scale jet properties based on the inferred mean proper motion, including a bulk Lorentz factor, jet inclination angle, projected position angle, intrinsic half opening angle and a mean 2−8 GHz spectral index of 0.31. The jet model is applied to predict quasi-periodic oscillations of ∼ 10 days, power law power spectrum shape and a contribution of up to ∼ 53 percent to the observed variable core flux density.

In the *unique* observations of 3C345.3 (Gupta *et al.* 2017), it is required to explain the systematic changes in the EVPA and in the polarization fraction. The key point of the helical model is to take advantage of GR effects when the source is close to the black hole and the bend is invoked to explain the optical EVPA variation and the bend in field shape and exploit the helical path to explain the degree of polarization variation as well similar to earlier models. The effect of GR is in modulating the Doppler factor as well as light bending it exits from the BH environment and the relativistic factor for time interval ratio between the observer and the source frame can be significant. Even if we ignore the GR effects, the shape of the magnetic surface and the helical path can be sufficient to produce the observed profiles.

4. On the degree of polarization

The EVPAs for the jet linear polarization with respect to jet direction for quasars tend to have polarization orthogonal to the jet, and for BL Lac objects, parallel to the jets (Marscher *et al.* 2002). The shock mechanism will likely produce polarization along the jet if it is a transverse shock. Since shocks are transient events, the polarization direction may not be constant over extensive lengths. Given that oblique internal shocks are also possible, a bimodal distribution of the relative EVPAs is not likely; the EVPAs in BL Lac seem to be in disagreement with the shock model. An alternative model of a relativistic jet carrying helical magnetic fields can both reproduce the average properties of the jet polarization, such as the bimodal distribution of the observed EVPAs.

The behavior of the observed degree of polarization for optically thin synchrotron emission with helical magnetic fields can be calculated using the standard formula

$$\Pi_t = \Pi_{\max} \sin^2 \chi', \quad (8)$$

where χ' is the viewing angle in the jet rest frame and is related to the observed viewing angle χ through the usual Lorentz transformation

$$\sin \chi' = \frac{\sin \chi}{\Gamma(1 - \beta \cos \chi)}. \tag{9}$$

One can vary Γ or χ and reproduce the observed polarization of the segment as shown by Raiteri *et al.* (2013).

If variability arises by the transverse shock wave model, the observed fractional polarization of the shocked plasma radiation was calculated by Hughes *et al.* (1985) as

$$\Pi_s \approx \frac{\alpha + 1}{\alpha + 5/3} \frac{(1 - k^{-2}) \sin^2 \chi'}{2 - (1 - k^{-2}) \sin^2 \chi'}, \tag{10}$$

where $(\alpha + 1)/(\alpha + 5/3)$ is the synchrotron polarization factor due to a relativistic electron population with particle distribution $dN/dE \propto E^{-p}$, with $p = 2\alpha + 1$, k is the degree of compression of the shock wave. Depending on the variation of Γ or $\chi_{\min}$ (similarly to the helical jet model) one can also possibly explain various observed properties including the anti-correlation between flux and polarization.

Based on the above construction, one can calculate Π as a function of trajectory and for transverse shocks when the EVPA is known. While the full model with GR effects for a helical trajectory and the polarization theory is complicated, here we consider a special relativistic treatment in cylindrical geometry. Next, we work out the details of EVPA for the case of the helical blob moving in a magnetic helix.

5. Time-dependent polarization model with a double helix

We need to explain the systematic changes in the EVPA and in the polarization fraction. The key is to take advantage of relativistic effects when the source is close to the black hole and the helical bend to explain the optical EVPA variation and to explain the degree of polarization variation. As a first consideration, if we treat the blob as a sphere (of charge Q) that is flowing along the helical magnetized structure, then the general expression for energy per solid angle per unit frequency in special relativistic limit as given in standard synchrotron theory as (e.g. Rybicki & Lightman 1986)

$$\frac{dW}{d\omega d\Omega} = \frac{Q^2 \omega^2}{4\pi^2 c^2} \left| \int \left[\mathbf{n} \times (\mathbf{n} \times \boldsymbol{\beta}) \kappa^{-3} \right] \right.$$
$$\left. \times \exp(-i\omega t) dt \right|^2 \tag{11}$$

where $\kappa = 1 - \mathbf{n} \cdot \boldsymbol{\beta}$ and $\mathbf{n}$ is the direction towards the observer. The trajectory of $\boldsymbol{\beta}$ given in MM15. The energy expression can be broken into parts $W_\parallel$ and $W_\perp$ using

$$\mathbf{n} \times (\mathbf{n} \times \boldsymbol{\beta}) = -\boldsymbol{\epsilon}_\perp \sin(c\beta t'/\varpi) + \boldsymbol{\epsilon}_\parallel \cos(c\beta t'/\varpi) \tag{12}$$

where $t' = t - R(t)/c$ is the retarded time, $\varpi(t')$ is the local radius of curvature and hence the polarization components can then be evaluated. If the path is not a standard helix, one has to start with the formulae from first principles.

Another approach, involves taking a blob equivalent to that of a min-jet having a constant rest frame emission and polarization properties that is following a bent helical path. The EVPA can be calculated from the trajectory from (Lyutikov *et al.* 2005)

$$\cos \tilde{\psi} = \mathbf{e} \times (\mathbf{n} \times \mathbf{l}) \quad \text{and} \quad \sin \tilde{\psi} = \mathbf{n} \times \mathbf{l} \tag{13}$$

where the angle is derived from the magnitude of the resulting vectors, $\mathbf{e}$ is the electric field direction, $\mathbf{l}$ is a unit normal to the plane containing $\mathbf{n}$ and a reference direction taken to be the projection of the jet axis to the plane of the sky [see Fig. 2; also see Fig. 2 of Lyutikov *et al.* (2005)].

We write the distribution function of the particles co-moving with the jet that is isotropic in momentum and power-law in energy as

$$dn = K_e \epsilon^{-p} d\epsilon dV d\Omega_\mathbf{p}. \tag{14}$$

The Stokes parameters per unit jet length for a steady flow can be written as (see Lyutikov *et al.* 2003)

$$I = \frac{p + 7/3}{p + 1} \frac{\kappa(\nu)}{D^2 (1 + z)^{2 + (p-1)/2}}$$
$$\int \frac{dS}{\sin \theta} K_e \, \mathcal{D}^{2 + (p-1)/2} |B' \sin \chi'|^{(p+1)/2}, \tag{15}$$

$$Q = \frac{\kappa(\nu)}{D^2 (1 + z)^{2 + (p-1)/2}}$$
$$\int \frac{dS}{\sin \theta} K_e \, \mathcal{D}^{2 + (p-1)/2} |B' \sin \chi'|^{(p+1)/2} \cos 2\tilde{\chi}, \tag{16}$$

$$U = \frac{\kappa(\nu)}{D^2 (1 + z)^{2 + (p-1)/2}}$$
$$\int \frac{dS}{\sin \theta} K_e \, \mathcal{D}^{2 + (p-1)/2} |B' \sin \chi'|^{(p+1)/2} \sin 2\tilde{\chi}, \tag{17}$$

$$V = 0. \tag{18}$$
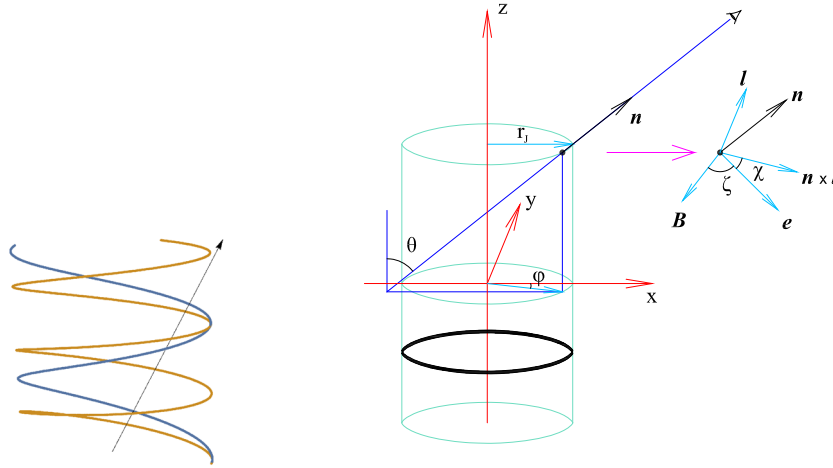
Figure 2. Left: The velocity helix and the magnetic helix have different pitches and the arrow indicates the direction towards the observer. Right: The figure shows the mini-jet in many forms of the blob, ring and a hollow cylinder. The location of the blob is given by the cylindrical coordinates $(r_J; \phi; z)$, the inclination angle is θ and at this location, the relative directions of the electric field direction, **e**, and the magnetic field direction **B** are indicated with respect to each other, the observer and a direction **l** that is normal to the plane containing $\hat{z}$ and **n**.

where D is the luminosity distance, the function $\kappa(\nu)$ is

$$\kappa(\nu) = \frac{\sqrt{3}}{4} \Gamma_E \left(\frac{3p-1}{12} \right) \Gamma_E \left(\frac{3p+7}{12} \right)$$

$$\frac{e^3}{m_e c^2} \left[\frac{3e}{2\pi m_e^3 c^5} \right]^{(p-1)/2} \nu^{-(p-1)/2}. \quad (19)$$

where Γ_E is the Euler-gamma function and the special relativistic Doppler boosting factor is

$$\mathcal{D} = \frac{1}{\Gamma(1 - \beta \cos \theta)}, \quad (20)$$

and $\tilde{\chi}$ is defined as the observed EVPA in the plane of the sky seen by the observer, measured clockwise from a fixed direction and is calculated below. The unit vector **l** is normal to the plane containing **n** and the reference direction in the plane of the sky, so that $\mathbf{l} = \{0, 1, 0\}$. Then,

$$\cos \tilde{\chi} = \hat{\mathbf{e}} \cdot (\mathbf{n} \times \mathbf{l}), \quad \sin \tilde{\chi} = \hat{\mathbf{e}} \cdot \mathbf{l}, \quad (21)$$

where $\hat{\mathbf{e}}$ is a unit vector in the direction of the electric field [see Lyutikov *et al.* 2003, 2005 (eqns C1–C8)]

$$\hat{\mathbf{e}} = \frac{\mathbf{n} \times \mathbf{q}}{\sqrt{q^2 - (\mathbf{n} \cdot \mathbf{q})^2}}, \quad (22)$$

$$\mathbf{q} = \hat{\mathbf{B}} + \mathbf{n} \times (\mathbf{v} \times \hat{\mathbf{B}}). \quad (23)$$

The shell is seen at an angle θ with respect to its axis, so that

$$\mathbf{v} = \beta\{\cos \phi, \sin \phi, w\}/\sqrt{1 + w^2} \quad (24)$$

$$\mathbf{n} = \{\sin \theta, 0, \cos \theta\} \quad (25)$$

and **B**′ in the emitting shell in the jet frame is helical

$$\mathbf{B}' = B'\{- \sin \psi' \sin \phi, \sin \psi' \cos \phi, \cos \psi'\}, \quad (26)$$

where ψ' is the magnetic field pitch angle in the shell rest frame. Due to relativistic aberration the observed electric field is not orthogonal to the observed **B** field and to its projection on the sky (Blandford & Königl 1979)

$$\mathbf{e} \cdot \mathbf{B} = (\mathbf{v} \times \mathbf{B}) \cdot (\mathbf{n} \times \mathbf{e}). \quad (27)$$

The angle between $\hat{\mathbf{e}}$ (which lies in the plane of the sky) and $\hat{\mathbf{B}}$ is given by

$$\cos \zeta = \hat{\mathbf{e}} \cdot \hat{\mathbf{B}} = \frac{(\hat{\mathbf{B}} \cdot \mathbf{n})(\hat{\mathbf{B}} \cdot (\mathbf{n} \times \mathbf{v}))}{\sqrt{q^2 - (\mathbf{n} \cdot \mathbf{q})^2}} \quad (28)$$

The DOP is given by $\Pi = \sqrt{Q^2 + U^2}/I$, and the resultant EVPA measured by the observer, $\tilde{\chi}_{res}$, is obtained from

$$\cos 2\tilde{\chi}_{res} = \frac{Q}{\sqrt{Q^2 + U^2}}, \quad \sin 2\tilde{\chi}_{res} = \frac{U}{\sqrt{Q^2 + U^2}},$$

$$0 \le \tilde{\chi}_{res} < \pi. \quad (29)$$

If emission geometry is a cylindrical shell, then the degree of polarization (DOP) becomes (Lyutikov *et al.* 2005)

$$\Pi = \frac{p+1}{p+7/3} \cos 2\tilde{\chi}. \quad (30)$$

Now we consider a mini-jet where the emission comes from a cylindrical shell whose EVPA angle works out to be

Table 2. Parameters for the jet simulations.

Run #	w	Γ	ψ'	θ
1	4	13	1.16	0.857
2	1.97	5.29	-0.773	1.07
3	1.97	5.29	0.773	1.07
4	2.52	6.76	0.427	0.606

The jet runs with parameters representing the velocity pitch angle arctan $(w/\sqrt{w^2+1})$, the bulk Lorentz factor Γ, ψ' is the magnetic pitch angle in the shell rest frame and θ is the inclination angle to the observer.

$$\cos\tilde{\chi}(\phi, \beta, w, \psi') = -\frac{\sqrt{1-\beta^2}\sin\theta\cos\psi'}{\sqrt{1-\beta^2\cos^2\psi'}}$$
$$-\frac{\cos\theta\sin\psi'\sin\phi}{\sqrt{1-\beta^2\cos^2\psi'}} + \frac{\beta\sqrt{1-\beta^2}\cos\psi'\cos\phi}{\sqrt{w^2+1}\sqrt{1-\beta^2\cos^2\psi'}}$$
$$+\frac{\beta w\sin\psi'\sin\phi}{\sqrt{w^2+1}\sqrt{1-\beta^2\cos^2\psi'}} \quad (31)$$

The formula for ζ is found to be

$$\cos\zeta(\phi, \beta, w, \psi') = \frac{\beta}{\sqrt{w^2+1}\left(\beta^2\cos^2\psi'-1\right)} \cdot$$
$$\left\{ -\sqrt{1-\beta^2}\cos^2\theta\sin\psi'\cos\psi' \right.$$
$$+ \sin\theta\cos\theta\left(\sin\phi\left[(\beta^2-1)\cos^2\psi'\right.\right.$$
$$\left.+\sin^2\psi'\right] + \sqrt{1-\beta^2}w\sin\psi'\cos\psi'\cos\phi\Big)$$
$$+\sin^2\theta\sin\psi'\sin\phi$$
$$\left(\sqrt{1-\beta^2}\cos\psi'\sin\phi - w\sin\psi'\cos\phi\right)\right\} \quad (32)$$

The EVPA angle eq. (31) is used to calculate the DOP using eq. (30) while the Doppler factor representing the

light curve is given by eq. (20) and the angle ζ between the observed E and B field is given by eq. (28).

We summarize our key results from the simulations carried out for the parameters given in Table 2.

1. The various runs given in Table 2, are shown in Figs. 3–5 showing correlation and anti-correlations between flux, DOP, and EVPA. The observed variations to a large extent can be explained by the double helix special relativistic model. Figure 3 is representative of an increasing DOP and decreasing flux as observed in Gaur *et al.* (2014), Fig. 4 is representative of a decreasing flux with increasing EVPA case as in Marscher *et al.* (2008), while Fig. 5 is representative of a decreasing flux and EVPA case seen by Abdo *et al.* (2010). Although the variation is shown for phase period of 2π, it is likely that the min-jet will last only for a fraction of the orbital period.
2. The key parameters identified from simulations are the relative pitch between the velocity and magnetic helices, the inclination angle, and the bulk Lorentz factor.
3. This encourages us to take the next step of building polarization model for a GR trajectory based on MM15 that takes advantage of GR effects when the source is close to the black hole can explain the optical PA variation. It will also exploit the helical path to explain the DOP variation that lasts for a short time.

The advantage of the method given in (Lyutikov *et al.* 2003, 2005) is the Lorentz transformation of the rest frame fields to the observed frame for the purposes of calculating the EVPA, $\tilde{\chi}$, and the angle between the electric and magnetic fields, ζ. This approach simplifies
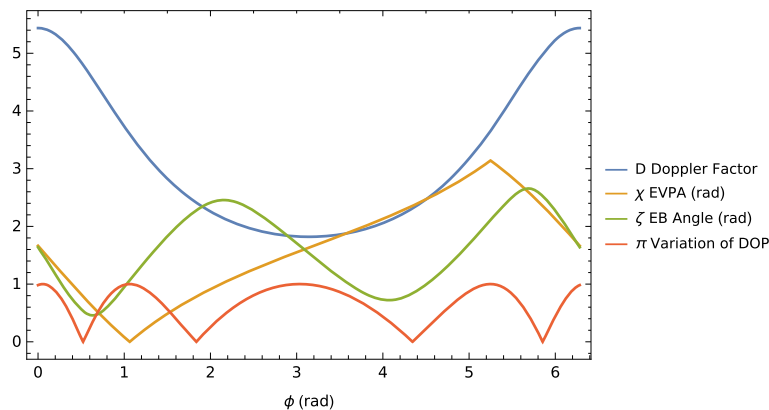
Figure 3. The case of flux increase and DOP increase with decrease in EVPA for parameters of run 1 given in Table 2.
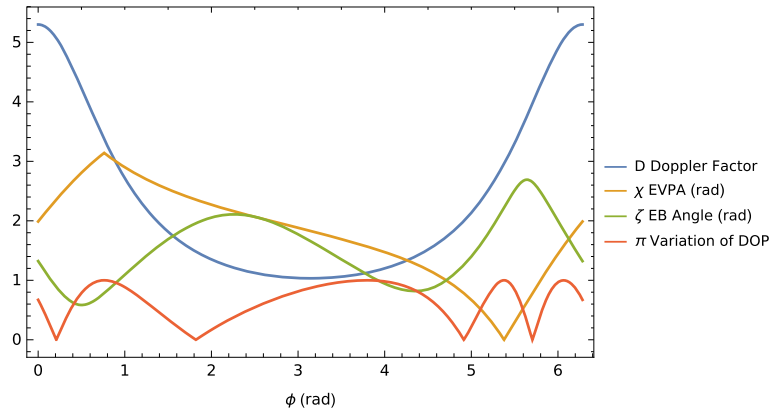
Figure 4. The case of flux decrease and DOP decrease with increase in EVPA for parameters of run 2 given in Table 2.
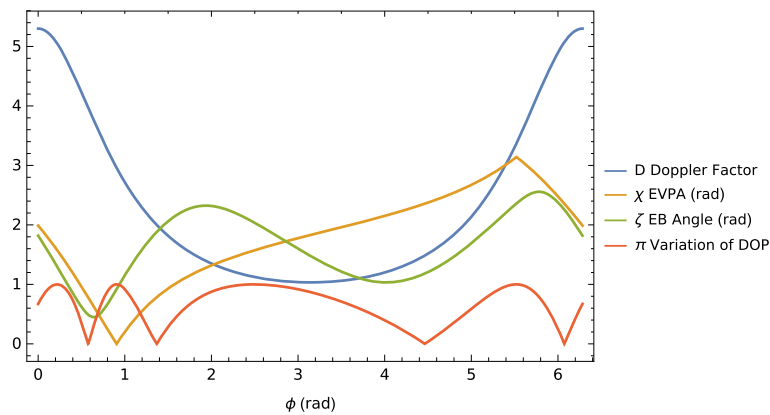
Figure 5. The case of flux decrease and DOP decrease with decrease in EVPA for for parameters of run 3 given in Table 2.
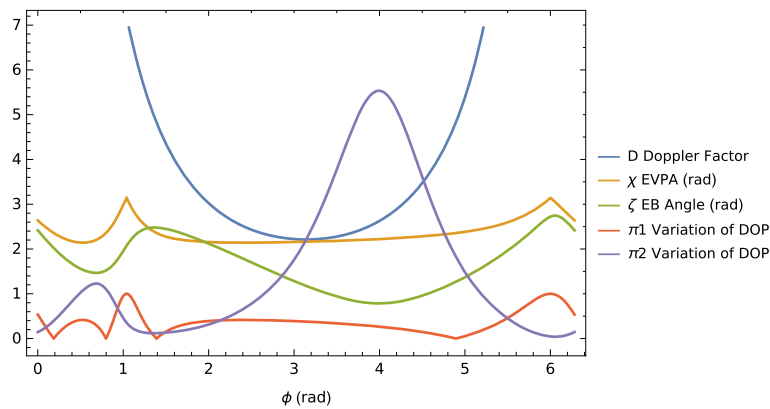
Figure 6. DOP variation for a ring π_1 as calculated from eq. (30) compared with that of a blob π_2 calculated from eq. (9) shown for parameters of run 4 given in Table 2.

the key step of Lorentz transformation of the emitted EM wave to the observer frame at a given instant where the changes are taking place over the timescale of the blob orbital motion.

The difference between steady versus transient polarization can be addressed by the geometry of the entity that is motion, specifically whether it is blob, ring or mini jet. If we take the blob to be equivalent to a mini-jet having a constant rest frame emission and polarization properties that is following a bent helical path, the resulting behavior of the observed degree of polarization for optically thin synchrotron emission with helical magnetic fields can be calculated using eq. (8), where χ' is the viewing angle in the jet rest frame

and is related to the observed viewing angle χ through the Lorentz transformation given by eq. (9). In case of a ring or a cylinder, the emission is azimuth averaged and the DOP calculated using eq. (30) will be flatter, as seen in Fig. 6.

The other issue is one of the kinematics and velocity field geometry; it is shown here that the assumption of a helix produces the desirable feature of flux variation. The choice of the magnetic field geometry also matters as it could be diverging like a cone or converging into a funnel; it results in variations in the polarization properties (averaging over azimuth and jet length).

6. Pulse profile from a helical jet or disk

We calculate the harmonics of a generic pulse profile of a helical jet or a disk. The observed flux is given by $S = D^{3+\alpha} S_0$ where the Doppler factor is given by eq. (2) where the angle between the velocity vector and the line of sight is given by

$$\beta \cos \xi = \frac{\hat{\mathbf{n}} \cdot \mathbf{v}}{|\mathbf{v}|} = \beta_\perp \cos(\phi + \phi_0) \sin i + \beta_\parallel \cos i. \quad (33)$$

The time interval as measured in the observer's frame $d\tilde{\tau}$ is related to the instantaneous rest frame $d\tau$ by $d\tilde{\tau} = D^{-1} d\tau$ and hence is related to the coordinate time interval dt. The factor D includes GR effects operating such as light bending, aberration, time delay, gravitational redshift, Doppler and relativistic beaming for QPOs in black hole systems (MM15).

We write the Doppler Fourier series of the pulse profile from a spot of a rotating object as a cosine series, including effects like Doppler boost, relativistic aberration, gravitational redshift and light bending in Schwarzschild geometry as

$$\frac{1}{(1 + \beta_\Gamma \cos \xi)^{3+\alpha}} = \sum_{n=0}^{\infty} C_n \cos n\phi, \quad (34)$$

where the coefficients are obtained from

$$C_n = \frac{1}{\pi} \int_{-\pi}^{\pi} \frac{\cos n\phi}{(1 + \beta_\Gamma \cos \xi)^{3+\alpha}} d\phi. \quad (35)$$

The resulting flux profile can be written as

$$F(\phi) \approx C_0 + C_1 \cos(\phi + \phi_0) + C_2 \cos[2(\phi + \phi_0)] + C_3 \cos[3(\phi + \phi_0)]. \quad (36)$$

We find for $\cos \xi = a_0 \cos(\phi + \phi_0) + b_0$ that

$$C_n = 2\pi(-a_0 + b_0 + 1)^p \, {}_3\tilde{F}_2 \left(\frac{1}{2}, 1, -p; 1 - n, n + 1; \frac{2a_0}{a_0 - b_0 - 1} \right), \quad (37)$$

where ${}_3\tilde{F}_2$ is the Hypergeometric PFQ regularized function, $a_0 = \beta_\perp \sin i$, $b_0 = \beta_\parallel \cos i$ and $p = -(3 + \alpha)$, where α is power law index of the emitted spectrum. It is found that the Cs are of order unity but it clearly depends on the source viewing angle and velocity vector of the jet. The fundamental frequency of the signal scaled for BHXRB will be given by

$$\nu_\phi = \frac{32.4}{(M/M_\odot)(r_J^{3/2} \pm a)} \text{kHz}. \quad (38)$$

Taking typical median values for the mass $M/M_\odot = 7$, $a = 0.3$, and $\nu = 6 - 30$ Hz, we infer a typical radius of the helix to be in the range 30–80 gravitational radii. The Type B QPOs are in the range 1–3 Hz and 6 Hz (Motta 2016; Casella *et al.* 2005) and are associated with relativistic jets. The Type C QPOs range between few mHz to about 10 Hz and can reach 30 Hz (Motta 2016 and references therein) and may be associated with jets (Kalamkar *et al.* 2016) but are more likely to be associated with hot flows during the outburst phase in the inner disc (Ingram *et al.* 2009; Poutanen *et al.* 1997). The derived orbital harmonics are however applicable to both situations.
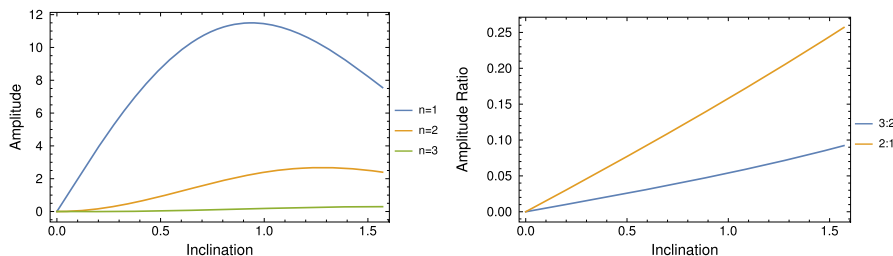
Figure 7. A plot of the amplitude of the fundamental modes (left) and the amplitude ratios as a function of inclination in radians (right) that can be compared with observations; here $\Gamma = 5$, $\alpha = 0$ and the pitch angle was 0.6 radians.

For Blazars, the typical time period turns to out be

$$T = 30.93\pi (r_J^{3/2} + a)(1 + z)m_6 s, \tag{39}$$

where z is the red shift of the source and $m_6 = M_\odot/(10^6 M_\odot)$.

We show in Fig. 7 the run of the amplitude and amplitude ratios of the lower harmonics as a function of the inclination angle. The ratios of the harmonics can be used to model the parameters like the inclination angle θ, Γ, and the pitch angle of the helical motion. Polarization models can complement this to identify the physical parameters if measurements of the degree of polarization and EVPA are available.

7. Conclusions

Using the double helix model (where both the velocity and magnetic field are helices), we have shown that for typical range we can reproduce the kind of behavior seen in observations. The key parameters involved in determining the behavior are Γ, θ and ζ, the relative pitch angle difference between the magnetic field and the velocity field. The scenario here is to have a helical path of the mini-jet (a part of a jet) in a helically shaped field. This is a reasonable assumption; as in MHD, this situation is consistent and allowed by Ferraro's law of isorotation, as the particles are moving on a common cylindrical and magnetic surface. The kinematic details of the relativistic MHD model is not given here but the general case is parametrized. The general assumption of a double helix provides a rich variety good enough to cover the observed cases. The geometry of the flow and the shape of the perturbation have natural consequences on the time profiles of the flux, DOP, and the EVPA. The transient nature of the event can be explained by the fact that the inhomogeneity changes from a blob into a ring or a cylinder as flows along and get into a shock; this can result in a variety of profiles and explain also the abrupt and sharp fall in the flux, over time scales shorter or close to the orbital periods.

The QPOs in black hole systems can be produced by the rotating blobs in the jet or in the disk. We have studied the harmonics of the QPO which last for about 0.1 s in BHXRBs and few minutes to hours in Blazars and variety of lower order harmonics can be simulated in this model. It is important to study the kinematics which is key to understanding both the flux and polarization profiles of EVPA and DOP. The next goal is to verify the models by fits to realistic flux and polarization data from BHXRBs and Blazars.

References

Abdo, A. A., Ackermann, M., Ajello, M. *et al.* 2010, Nature 463, 919

Aharonian, F., Akhperjanian, A. G., Bazer-Bachi, A. R. *et al.* 2007, Astrophys. J. Lett. 664, L71

Blandford, R. D., Königl, A. 1979, ApJ 232, 34

Bonning, E. W., Bailyn, C., Urry, C. M., *et al.* 2009, Astrophys. J. Lett. 697, L81

Böttcher, M., Marscher, A. P., Ravasio, M. *et al.* 2003, ApJ 596, 847

Camenzind, M., Krockenberger, M. 1992, Astron. Astrophys. 255, 59

Casella, P., Belloni, T., Stella, L. 2005, ApJ 629, 403

Fender, R. P., Homan, J., Belloni, T. M. 2009, Mon. Not. Roy. Astron. Soc. 396, 1370

Fender, R., Belloni, T. 2012, Science 337, 540

Gaur, H., Gupta, A. C., Strigachev, A. *et al.* 2012b, Mon. Not. Roy. Astron. Soc., 425, 3002

Gaur, H., Gupta, A. C., Wiita, P. J. 2012a, Astronom. J. 143, 23

Gaur, H., Gupta, A. C., Wiita, P. J. *et al.* 2014, Astrophys. J. Lett. 781, L4

Gupta, A. C., Mangalam, A., Wiita, P. J. *et al.* 2017, arXiv:1708.03504

Gopal-Krishna, Wiita, P. J. 1992, Astron Astrophys. 259, 109

Hovatta, T., Valtaoja, E., Tornikoski, M., Lähteenmäki, A. 2009, Astron. Astrophys. 494, 527

Hughes, P. A., Aller, H. D., Aller, M. F. 1985, ApJ 298, 301

Ingram, A., Done, C., Fragile, P. C. 2009, Mon. Not. Roy. Astron. Soc. 397, L101

Jorstad, S. G., Marscher, A. P., Larionov, V. M. *et al.* 2010, ApJ 715, 362

Kalamkar, M., Casella, P., Uttley, P. *et al.* 2016, Mon. Not. Roy. Astron. Soc. 460, 3284

Konigl, A., Choudhuri, A. R. 1985, ApJ 289, 188

Lachowicz, P., Gupta, A. C., Gaur, H., Wiita, P. J. 2009, Astron. Astrophys. 506, L17

Larionov, V. M., Jorstad, S. G., Marscher, A. P. *et al.* 2013, ApJ 768, 40

Li, X., Mohan, P., An, T. *et al.* 2018, ApJ 854, 17

Liu, B.-R., Liu, X., Marchili, N. *et al.* 2013, Astron. Astrophys. 555, A134

Liu, Y., Jiang, D. R., Gu, M. F. 2006, ApJ 637, 669

Lyutikov, M., Pariev, V. I., Blandford, R. D. 2003, ApJ 597, 998

Lyutikov, M., Pariev, V. I., Gabuzda, D. C. 2005, Mon. Not. Roy. Astron. Soc. 360, 869

Marscher, A. P., Jorstad, S. G., Mattox, J. R., Wehrle, A. E. 2002, ApJ 577, 85

Marscher, A. P., Jorstad, S. G., D'Arcangelo, F. D. *et al.* 2008, Nature 452, 966

Marscher, A. P., Jorstad, S. G., Larionov, V. M. *et al.* 2010, Astrophys. J. Lett. 710, L126

Mohan, P., Mangalam, A. 2014, ApJ 791, 74.

Mohan, P., Mangalam, A., Chand, H. *et al.* 2011, J. Astrophys. Astron. 32, 117.

Mohan, P., Mangalam, A. 2015, ApJ 805, 91 (MM15)

Mohan, P., An, T., Frey, S. *et al.* 2016, Mon. Not. Roy. Astron. Soc. 463, 1812

Motta, S., Homan, J., Muñoz Darias, T. *et al.* 2012, Mon. Not. Roy. Astron. Soc. 427, 595

Motta, S. E. 2016, Astronomische Nachrichten 337, 398

Poutanen, J., Krolik, J. H., Ryde, F. 1997, Mon. Not. Roy. Astron. Soc. 292, L21

Raiteri C. M. *et al.*, 2011, A&A 534, A87

Raiteri, C. M., Villata, M., D'Ammando, F. *et al.* 2013, Mon. Not. Roy. Astron. Soc., 2378

Rybicki, G. B., Lightman, A. P. 1986, Radiative Processes in Astrophysics, by George B. Rybicki, Alan P. Lightman, pp. 400. ISBN 0-471-82759-2. Wiley-VCH , June 1986., 400

Sasada, M., Uemura, M., Arai, A. *et al.* 2010, Pub. Astron. Soc. Jpn. 62, 645

Vercellone, S., Chen, A. W., Vittorini, V. *et al.* 2009, ApJ 690, 1018

Vercellone, S. *et al.*, 2010, ApJ 712, 405

Zhang, H., Chen, X., Böttcher, M., Guo, F., Li, H. 2015, ApJ 804, 58

Zhang, H., Chen, X., Böttcher, M. 2014, ApJ 789, 66